Ferromagnetism in inhomogeneous $Zn_{1-x}Co_xO$ thin films

Maureen Tay
Department of Electrical and Computer Engineering, National University of Singapore, 4 Engineering Drive 3, Singapore 117576, Singapore and Data Storage Institute, 5 Engineering Drive 1, Singapore 117608, Singapore

Yihong Wu[a)]
Department of Electrical and Computer Engineering, National University of Singapore, 4 Engineering Drive 3, Singapore 117576, Singapore

Gu Chang Han, Tow Chong Chong, and Yuan Kai Zheng
Data Storage Institute, 5 Engineering Drive 1, Singapore 117608, Singapore

Shi Jie Wang
Institute of Materials Research and Engineering (IMRE), 3 Research Link, Singapore 117602, Singapore

Yanbin Chen and Xiaoqing Pan
Department of Materials Science and Engineering, University of Michigan, H. H. Dow Building, 2300 Hayward Street, Ann Arbor, Michigan 48109-2136

(Received 1 December 2005; accepted 1 July 2006; published online 27 September 2006)

We report on a systematic study of structural, optical, electrical, and magnetic properties of $Zn_{1-x}Co_xO$ ($x=0.05-0.29$) thin films codoped with Al (<0.1%). Both codoped (in which Co is cosputtered with other elements) and δ-doped (in which Co is doped digitally in the host matrix) samples have been prepared and studied. Prior to doping of Co, growth conditions were optimized to produce ZnO:Al films with a resistivity of about 1.3 mΩ cm. Although all the films with x in the range of 0.05–0.29 showed clear hysteresis at room temperature in magnetometry measurement and absorption peaks associated with the *d-d* transitions of Co^{2+} ions, only the most heavily doped samples have shown clear anomalous Hall effect. The latter also showed strong, but photon energy dependent, magnetic circular dichroism and negative magnetoresistance at room temperature. These results in combination with detailed structural analysis by transmission electron microscope and x-ray diffraction study revealed that the ferromagnetic properties of $Zn_{1-x}Co_xO$ were mostly originated from secondary phases and Co precipitates. The influence of inhomogeneity on the interpretation of various measurement results is also discussed. © *2006 American Institute of Physics*. [DOI: 10.1063/1.2348632]

I. INTRODUCTION

ZnO-based diluted magnetic semiconductors (DMSs) have attracted great attention both theoretically and experimentally.[1] Despite a considerable effort aimed at elucidating the nature of ferromagnetism in ZnO-based magnetic semiconductors, its origin still is debatable. The mean-field Zener model of Dietl *et al.* [2] predicts a Curie temperature (T_C) above room temperature for ZnO doped with 5% Mn and with a hole concentration of 3.5×10^{20} cm^{-3}. Using the first-principles calculation, Sato and Katayama-Yoshida predict that V, Cr, Fe, Co, or Ni doped ZnO is a half-metallic double-exchange ferromagnet, Mn doped ZnO is an antiferromagnetic insulator which changes to a ferromagnet by additional doping of holes, whereas Ti or Cu doped ZnO remains paramagnetic.[3] It was also shown that electron doping stabilizes the ferromagnetic ordering of Fe, Co, or Ni doped ZnO.[4] The first-principles spin-density functional calculations by Lee and Chang predict that heavy electron doping and high Co concentration are required for obtaining ferromagnetism in ZnCoO.[5] On the other hand, Spaldin argues theoretically that only hole doping promotes ferromagnetism in both ZnCoO and ZnMnO.[6] Very recently, Sluiter *et al.* predict that both hole doping and electron doping promote ferromagnetic ordering in ZnCoO and ZnMnO.[7] Hydrogen-mediated spin-spin interaction was also predicted to be able to induce high temperature ferromagnetism in ZnCoO.[8] Similar to theoretical work, experimental investigations so far have also resulted in widely scattered data, ranging from intrinsic ferromagnetism with various Curie temperatures[1,9–15] to nonferromagnet[16–18] or ferromagnet with extrinsic origins.[1,19–25] The large disparity in the experimental results is caused by two major factors: (i) the properties of ZnCoO are very sensitive to the structure and chemistry at the nanoscale, which in turn strongly depend on preparation techniques and conditions, and (ii) most of the characterization techniques, be it magnetic, electrical, or optical, only probe a certain portion or aspect of the sample in either the spatial or energy domain; therefore, the combination of techniques which are commonly used to classify the origin of ferromagnetism in ZnO-based DMSs will only be valid when the samples are homogeneous.

In order to gain an understanding of how homogeneous and inhomogeneous samples differ in terms of magnetic,

[a)]Electronic mail: elewuyh@nus.edu.sg

electrical, and optical properties revealed by different characterization techniques, in this work, we have conducted a systematic study of $Zn_{1-x}Co_xO$ thin films fabricated by magnetron sputtering. Both codoped and δ-doped samples, in which the Co composition has been varied from 5 to 29 at. %, have been prepared and studied. As we will show later, the δ-doped samples contain both valence 2+ and 0 Co, whereas the codoped samples contain only Co^{2+} ions. In spite of the difference in valence of Co atoms, all the samples were found to exhibit ferromagnetic properties up to room temperature by magnetometry measurement. For codoped samples, the coercivity and saturation magnetization show a rapid increase with Co composition in the range of $x=15\%-20\%$, indicating the onset of formation of percolated magnetic regions in the samples. Above this Co composition range, both magnetic circular dichroism (MCD) and anomalous Hall effect (AHE) have been observed up to room temperature. However, the former was found to depend strongly on photon energy. These results in combination with detailed structural analysis confirmed that the ferromagnetism observed in our heavily doped samples was of extrinsic origin, originating from Zn incorporated CoO, $ZnCo_2O_4$, and/or Co clusters. Based on the results obtained, we will discuss how inhomogeneity affects the interpretation of various measurement data for inhomogeneous ZnCoO samples, which may help clarify some of the inconsistencies reported so far in this system.

II. EXPERIMENT

$Zn_{1-x}Co_xO$ ($x=0.05-0.29$) thin films were deposited on (0001) sapphire (α-Al_2O_3) substrates in a high vacuum chamber with a base pressure $<1\times10^{-7}$ Torr using a combination of radio-frequency (rf) and dc magnetron sputtering. Sintered ZnO, Al_2O_3, and Co materials were used as the sputtering sources for ZnO, Al, and Co, respectively. All samples were sputtered in an atmosphere of pure Ar gas at a pressure of 5 mTorr. Prior to deposition, substrates were cleaned using Ar reverse sputtering at 20 mTorr in the precleaning chamber. A series of experiments have been carried out to optimize the substrate temperature (room temperature to 600 °C) and sputtering powers for ZnO (50–200 W) and Al_2O_3 (20–50 W). At an optimal deposition condition of 500 °C substrate temperature, ZnO sputtering power of 150 W, and Al_2O_3 sputtering power of 30 W, ZnO:Al films with a resistivity of 1.3 mΩ cm were obtained. Under these conditions, the deposition rate of ZnO:Al was ~4.8 nm/min. Subsequently, Co was doped into ZnO:Al by using the above optimum deposition condition, while varying either the Co sputtering power from 3 to 32 W for codoped samples or the Co sputtering duration from 10 to 98 s for δ-doped samples. For the codoped samples, samples 1–4, Co was added to ZnO:Al by cosputtering Co with ZnO and Al_2O_3. On the other hand, in δ-doped samples, samples 5–8, Co was doped "digitally" into the ZnO:Al host matrix with nominal thicknesses of 0.1, 0.25, 0.5, and 1 nm, respectively. As the actual thicknesses might be different from the nominal ones because the latter were determined from the thickness of Co deposited at room temperature, in what follows we will use the Co sputtering durations instead of nominal thicknesses in our discussion of the second group of samples, which are 10, 25, 49, and 98 s, respectively. During each of the 60 repeating cycles, a ZnO:Al spacer with a thickness of about 2.38 nm was deposited, each followed by the deposition of a Co layer. The thickness of Co was chosen such that the average Co composition will be roughly the same as those of the aforementioned four codoped samples. The actual Co compositions measured by x-ray photoelectron spectroscopy were 0.046, 0.137, 0.198, and 0.287 for codoped samples 1, 2, 3, and 4, respectively. Table I lists the details of the samples under this study. The microstructures and chemical compositions of these samples were characterized using x-ray diffraction (XRD), high-resolution transmission electron microscopy (HRTEM), and electron energy-loss spectroscopy (EELS). The optical and magneto-optical properties of the samples were characterized using a UV-visible spectrophotometer and by MCD measurement, respectively. The magnetic properties of the sample were characterized using a commercial superconducting quantum interference device (SQUID) magnetometer. For electrical characterization, Hall bars with a length of 324 μm and a width of 80 μm were fabricated for each sample using a direct laser writer. A 1-3-3-1 eight-contact Hall bar configuration was used to measure both the longitudinal and Hall voltages. The same sample geometry has also been used to measure the magnetoresistance (MR).

TABLE I. Details of the samples under study.

Sample number	Co doping technique	Sputtering power or duration	Co composition or sample structure
1	Codoping	3 W	$Zn_{1-x}Co_x$:Al ($x=0.046$)
2		8 W	$Zn_{1-x}Co_x$:Al ($x=0.137$)
3		16 W	$Zn_{1-x}Co_x$:Al ($x=0.198$)
4		32 W	$Zn_{1-x}Co_x$:Al ($x=0.287$)
5	δ doping	10 s	[ZnO:Al(2.38 nm)/Co(0.1 nm)]×60
6		25 s	[ZnO:Al(2.38 nm)/Co(0.25 nm)]×60
7		49 s	[ZnO:Al(2.38 nm)/Co(0.5 nm)]×60
8		98 s	[ZnO:Al(2.38 nm)/Co(1.0 nm)]×60

III. RESULTS AND DISCUSSION

A. Structural properties

For samples 1–3 and 5–7, the XRD patterns in the range of $20°<2\theta<90°$ mainly show the existence of ZnO diffraction peaks. However, for sample 4, in addition to ZnO-related peaks, we have also observed a weak and broad peak at $2\theta\sim43°-48°$, which covers the range of (111) peak for Co (44.217°), (400) peak for $ZnCo_2O_4$, (44.74°), (400) peak for Co_3O_4 (44.81°), and (102) peak for ZnO (47.539°). Therefore, it is difficult to conclude which phase is responsible for this broad peak by XRD data alone. On the other hand, clear peaks have been observed at 44.4°–44.76°, 50.5°, and 51.1° for sample 8, which are near those of the (111) and (200) peaks of Co at 44.217° and 51.524°, respectively. According to literature, using x-ray diffraction,[10,26] the solubil-

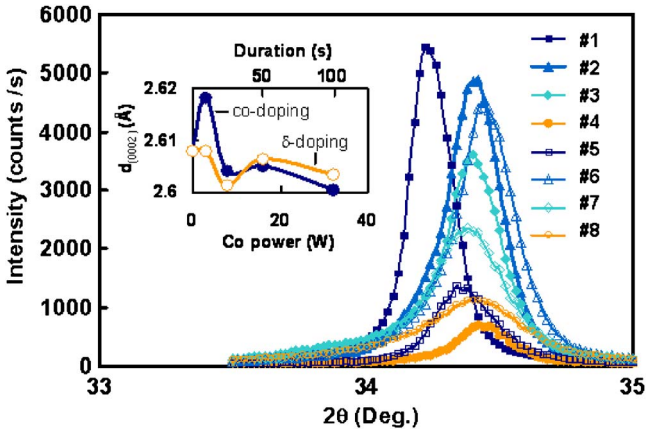

FIG. 1. (Color online) XRD patterns of both codoped and δ-doped samples on Al_2O_3 substrate [the insert shows the d spacing for ZnO (002) peaks at various cobalt doping levels].

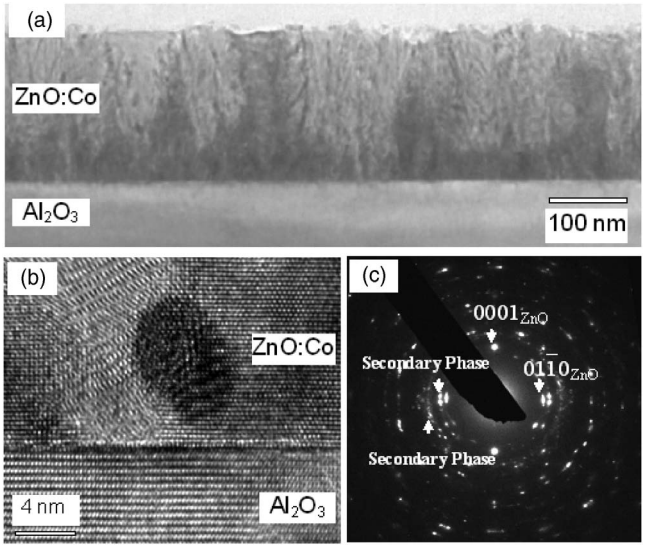

FIG. 2. (a) Cross-sectional TEM image of sample 4. (b) HRTEM image of a selected region showing the existence of an impurity phase and (c) electron diffraction pattern of the same region showing the existence of secondary phases ($ZnCo_2O_4$ and/or CoO).

ity limit of Co in ZnO is found to be about 25%, below which, in principle, Co can be doped homogeneously in ZnO, whereas above this limit the formation of secondary phase and precipitates is expected. We would thus expect samples 4 and 8 to contain secondary phases or clusters. We will come back to this again shortly when we discuss the transmission electron microscopy (TEM) results. Figure 1 shows the XRD patterns in the region near the (0002) diffraction peak for the two groups of samples. As can be seen from the insert of the figure, the lattice constant along the c axis initially increases with the Co doping level, then decreases at higher doping levels. This is in sharp contrast to the results reported[9,27] which showed that the lattice constant increases linearly with Co composition. However, our results are very similar to those of Lee *et al.*, which showed that the lattice constant increases linearly when $x<0.2$, above which it starts to decrease.[10] Prellier *et al.* have also observed a plateau for $x>7\%$ after the initial increase of lattice constant with the Co composition.[28] The discrepancy might be caused by various factors including sample preparation techniques and conditions, position of Co atoms in the ZnO lattice and their coordination numbers, valence of Co ions, and formation of secondary phases. The results shown in Fig. 1 can be understood as follows.[29] As the ionic radius of Co^{2+} is about 96% of that of Zn^{2+}, the in-plane lattice constant of relaxed ZnCoO film is expected to decrease when the Zn atoms are replaced by Co atoms, leading to an increase of out-of-plane lattice constant due its large Poisson ratio. However, with the further increase of Co composition, it is plausible that, in addition to substitutional sites, Co may also start to occupy interstitial sites due to the deformation of lattice structures caused by the substitution of nearby zinc atoms by other Co atoms. This will result in an increase of in-plane lattice constant and shrinkage of out-of-plane lattice constant. The actual mechanism might be more complex in heavily doped samples because of the formation of secondary phases and inhomogeneity of the sample as revealed by the HRTEM.

Figure 2(a) is a TEM image of sample 4. Columnar growth, similar to that observed by Schaedler *et al.*,[30] is observed. Figure 2(b) shows a HRTEM image of a region near the interface between the thin film and the substrate. Nano-sized secondary phases are frequently observed, as shown by a dark particle in Fig. 2(b). Figure 2(c) is the selected area electron diffraction of the region corresponding to Fig. 2(b), which shows the existence of possibly $ZnCo_2O_4$ and/or CoO phase in the film. Electron energy-loss spectroscopy confirms that the valence state of Co is 2+ in codoped samples, indicating that the inhomogeneity does not come from clustering of Co atoms in these samples. In comparison, the δ-doped samples (samples 6 and 8) showed a variation of 0 and 2+ valence states at different positions of the sample. These results along with the electron and x-ray diffraction data confirm that the δ-doped samples contain both substitutional Co and Co clusters, whereas the codoped samples are mainly embedded with secondary phases.

B. Optical properties

Figures 3(a) and 3(b) show the transmission spectra for codoped and δ-doped samples, respectively. Also shown in these figures are the transmission spectra of ZnO:Al films. In order to eliminate the influence of differences in sample surface condition and thickness, transmittance is normalized to the value of 800 nm. A sharp decrease of transmittance occurs at 384 nm for the ZnO:Al sample, which corresponds to the band edge absorption. A clear redshift of band edge absorption is observed in the codoped samples, which increases with increasing the Co composition. However, in addition to the redshifted absorption edges, samples 1–3 also show a blueshifted band edge as compared to ZnO:Al samples. Yoo *et al.*[29] and Kim and Park[27] argue that the redshift is mainly due to *sp-d* exchange interactions between band electrons and localized d electrons of the Co^{2+} ions substituting for Zn ions. The *s-d* and *p-d* exchange interactions give rise to a negative and a positive correction to the conduction- and valence-band edges, respectively, leading to shrinkage of the band gap. However, this may not apply to the case here because of the high concentration of Co. The large redshift

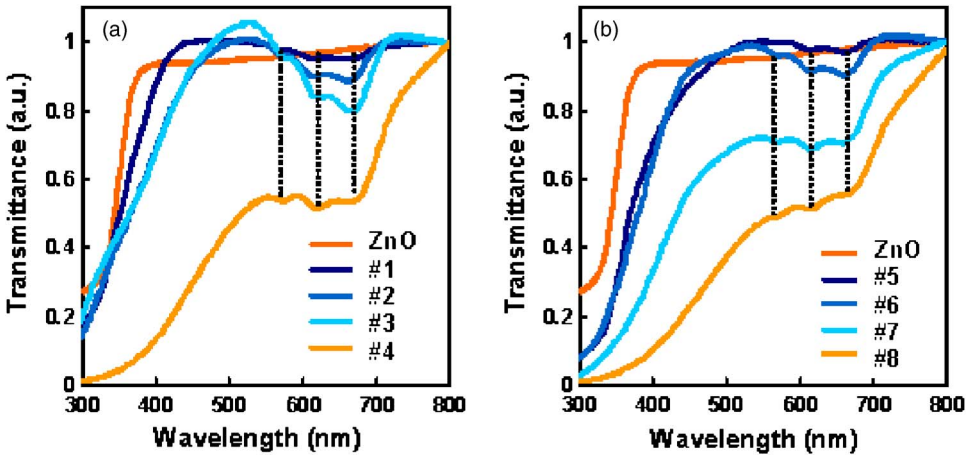

FIG. 3. (Color online) Optical transmission spectra of (a) cosputtered and (b) δ-doped samples.

could be considered as being caused by the formation of secondary phases such as $ZnCo_2O_4$ and CoO.[31] The blueshift might be caused by the biaxial compressive strain in ZnCoO, as shown by the XRD data. In addition to the band edge absorption, absorption bands were also observed for all samples at 571, 618, and 665 nm, which are attributed to d-d transitions of tetrahedrally coordinated Co^{2+}. They are assigned as ${}^4A_2(F) \rightarrow {}^2A_1(G)$, ${}^4A_2(F) \rightarrow {}^4T_1(P)$, and ${}^4A_2(F) \rightarrow {}^2E(G)$ transitions in high spin state $Co^{2+}(d^7)$, respectively.[27,29,32] As can be seen from both Figs. 3(a) and 3(b), the absolute strength of these absorption bands increases almost linearly with increasing the Co composition, whereas the amplitude of the absorption fringes initially increases and then decreases with the increase of Co concentration. The former suggests that majority of Co atoms substitute for Zn to form $Co^{2+}(d^7)$ ions. The latter can be ascribed to the fluctuations in the local crystal field surrounding different Co ions, in particular, the formation of Co–Co bonds at very high Co compositions, in the formation of secondary phases or Co clusters. Although the overall shape of the transmission spectra for δ-doped sample is similar to that of codoped samples with the same nominal Co composition, the codoped samples tend be more transparent than their δ-doped counterparts, which might be caused by the formation of Co clusters in the latter, as confirmed by HRTEM observations.

C. Magnetic and magneto-optical properties

The magnetic properties of codoped samples, samples 1–3, and those of δ-doped samples, samples 5–7, are very weak, though clear hysteresis curves were observed for all the samples at 300 K. In sharp contrast to these samples, both codoped sample, sample 4, and δ-doped sample, sample 8, showed very strong ferromagnetic properties. In Fig. 4(a), we only show the in-plane magnetization (M) versus magnetic field (H) curves for samples 2, 3, and 4, respectively. As can be seen from the figure, the saturation magnetic moment for sample 4 is two orders of magnitude greater than those of the other two samples. This difference is substantial considering the fact that there is only a factor of 2–4 times difference in the Co composition among the three samples. Figures 4(b) and 4(c) show the dependence of coercivity and saturation magnetization, respectively, on the Co composition for codoped samples. A rapid increase of both coercivity and saturation magnetization was observed in the composition range of 20%–25%. This range agrees well with the onset composition of formation of secondary phases and Co clusters as revealed by the XRD and HRTEM measurements. Figure 4(d) shows the M-H curves of sample 4 at different temperatures both along and out of the plane. These curves show that the sample exhibits a well-defined perpendicular anisotropy,[33] which could be due to the formation of columnarlike structures observed in the TEM image [Fig. 2(a)]. The out-of-plane curves are sheared due to the shape anisotropy. Both field-cooled (FC) and zero-field-cooled (ZFC) curves showed that the Curie temperature of this sample is higher than 400 K. Similar to the XRD and optical transmission data described above, the group of δ-doped samples exhibits the same trend as that of the codoped samples, i.e., the saturation magnetization of sample 8 is much higher than those of samples 5–7, though the difference is not as much as in the case of codoped samples. The δ-doped samples also showed a lower M_s and smaller H_c as compared to the codoped counterparts with the same nominal Co compositions. The out-of-plane anisotropy of sample 8 is also not as obvious as that of sample 4. All these indicate again that the contribution of Co clusters to the magnetic properties is more prominent in δ-doped samples.

The magnetic properties of samples 2, 4, 6, and 8 were also studied by the MCD analysis.[34,35] The results are summarized as follows: (1) sample 2 was found to be paramagnetic down to 6 K; (2) samples 4 and 8 are ferromagnetic from 6 to 300 K, but the MCD signals are strongly dependent on the photon energy; and (3) sample 6 showed both paramagnetic and ferromagnetic MCD at 6 K, but only the ferromagnetic component was observed at 300 K. The MCD of sample 6 was found to be independent of the photon energy. However, the ferromagnetic signal of sample 6 is about 15 times weaker than those of samples 4 and 8. As we mentioned above, the SQUID measurement has shown that all the samples exhibit ferromagnetism at room temperature. The contradiction between SQUID and MCD data for sample 2 may be due to the fact that the sample size for SQUID measurement was much larger than the light spot size for MCD measurement or the MCD is insensitive to defect originated ferromagnetism. For sample 6, the low-

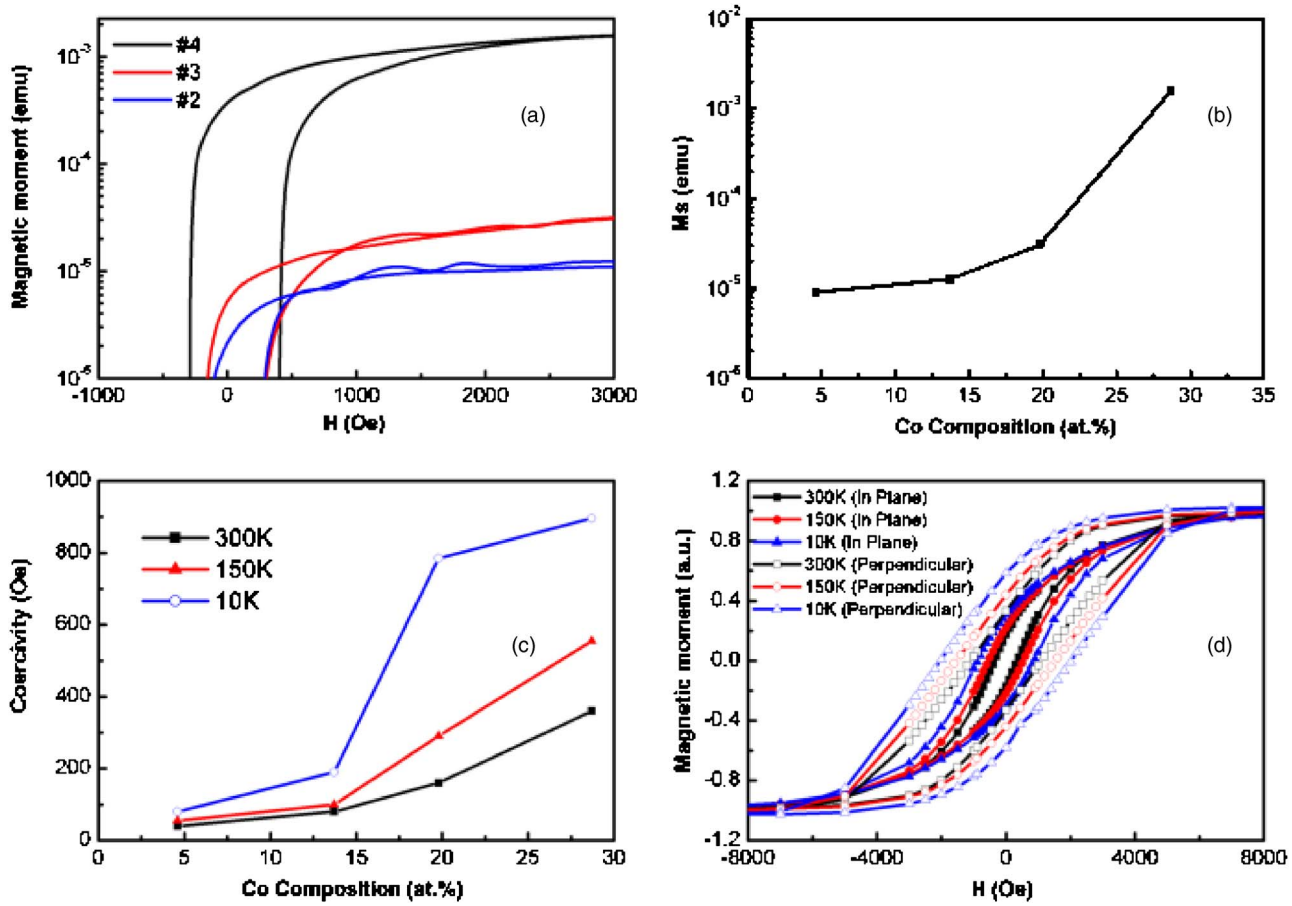

FIG. 4. (Color online) (a) In-plane *M-H* curves of codoped samples 2–4. (b) Coercivity as a function of Co composition for codoped samples at different temperatures. (c) Saturation magnetization as a function of Co composition for codoped samples at room temperature. (d) *M-H* curves of sample 4 measured at 10, 150, and 300 K (both in-plane and perpendicular to sample surface), respectively.

temperature paramagnetic phase may come from ZnCoO, while the high-temperature ferromagnetic phase is due to Co clusters which were observed by HRTEM. This agrees well with EELS results which have detected a mixture of 0 and 2+ valence states for Co in δ-doped samples. Figures 5(a) and 5(b) show the MCD hysteresis curves of sample 4 obtained at different photon energies at both 6 and 300 K. The MCD curves are strongly dependent on the photon energy. Similar results have also been obtained for sample 8 [Figs. 5(c) and 5(d)]. These results suggest that these samples are inhomogeneous and consist of ferromagnetic regions of different phases. For comparison, we have also shown the *M-H* curves measured by SQUID and Hall effect. In order to facilitate the comparison, the curves have been normalized to the magnitude in the *y* axis. We will come back shortly to discuss in detail the difference among the *M-H* curves after the Hall measurement results are presented.

D. Electrical transport properties

1. Temperature dependence of resistivity and differential conductance curve

Prior to deposition of Co-doped ZnO films, growth conditions were optimized to produce ZnO:Al films with a resistivity of about 1.3 mΩ cm. The resistivity of Co-doped films normally increases with Co concentration. Figure 6 shows the temperature-dependence of resistivity for both codoped and δ-doped samples with different Co concentrations. Although it is relatively insensitive to temperature, all samples but sample 4 exhibit weak metallic properties in the temperature range of 45–300 K. As has been revealed by TEM and MCD measurements, samples studied are inhomogeneous and consist of regions of different magnetic properties. Depending on the size, distribution, and density of the inhomogeneous regions, their effect should be reflected in transport properties, especially in differential conductance. The differential conductance curves for sample 4 are shown in Figs. 7(a) and 7(b), for the cases without and with an applied magnetic field of 4000 Oe, respectively. As can be observed in Fig. 7(b), the application of a magnetic field induces noise in the conductance curve. Also, the parabolic shape of the curve can be understood as being caused by spin-dependent tunneling between or across ferromagnetic regions.[36,37] This further confirms the inhomogeneity of this sample.

2. Magnetoresistance

Figure 8 shows the MR curves of sample 4 measured with a field in different directions: (i) perpendicular to plane, (ii) in-plane and along the current direction, and (iii) in-plane and perpendicular to the current direction. The observation of perpendicular anisotropy agrees well with SQUID measurement. The similarity between the two in-plane curves

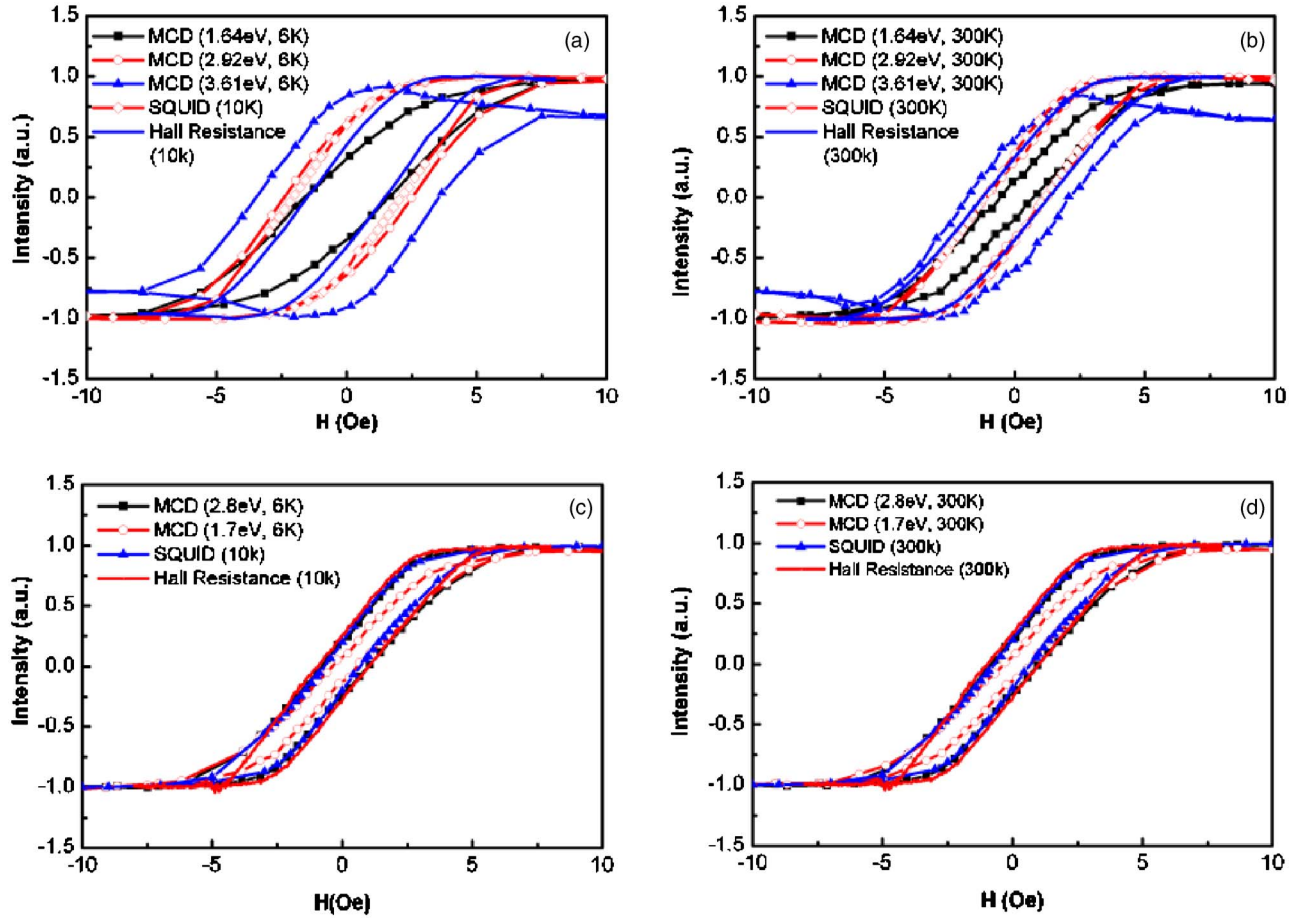

FIG. 5. (Color online) Hysteresis curves measured by SQUID, MCD, and Hall effect, respectively, for sample 4 at (a) low temperature and (b) 300 K, and sample 8 at (c) low temperature and (d) 300 K. All the curves are normalized to the magnitude in the y axis.

[cases (ii) and (iii)] and the observation of negative MR suggest that the sample is of granular nature. The observation of a larger coercivity in (iii) than that in (ii) implies that the ferromagnetic regions are either magnetically percolated or coupled magnetostatically. This explains why the magnetic properties of sample 4 is much stronger that those of samples 1–3. Negative MR of about 0.1% has been observed compared to the large 11% observed by Yan *et al.*[38] in their inhomogeneous ZnCoO magnetic semiconductor films. They attributed the large MR to spin-dependent hopping and magnetic-field-induced change in the localization length.

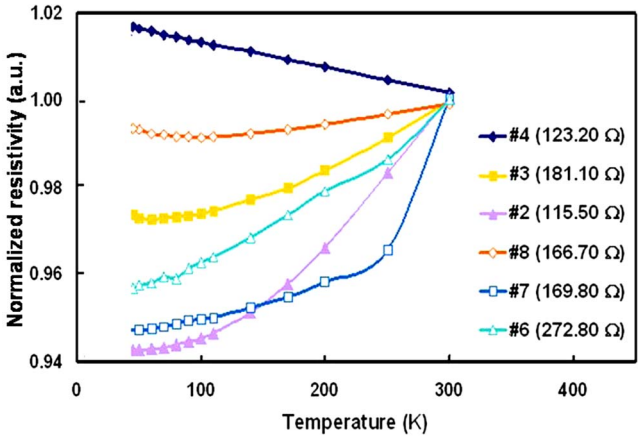

FIG. 6. (Color online) Normalized resistance as a function of temperature for both codoped and δ-doped samples. The legend shows the sheet resistance at room temperature.

3. Hall effect

The Hall effect of DMS is known to consist of both ordinary Hall effect (OHE) and anomalous Hall effect (AHE), and thus the Hall resistance is given by[39]

$$R_{\mathrm{Hall}} = \frac{R_0}{d}B + \frac{R_S}{d}M_{\perp},$$

where R_0 is the ordinary Hall coefficient, R_S is the anomalous Hall coefficient, d is the sample thickness, and $M_{\perp}$ is the magnetization of the sample in the vertical direction. R_S is proportional to R_{sheet}, the sheet resistance. The first term denotes OHE, while the second term is the contribution from AHE. In addition to III-V-based DMSs,[39,40] the AHE has also been observed in TiO_2:Co (Ref. 41) and Si-based systems[42] Although the presence of AHE was considered as one of the strong evidences for intrinsic ferromagnetism, caution should be taken for inhomogeneous systems, in particular, those containing ferromagnetic clusters. In fact, AHE has been observed in $TiO_{2-\delta}$ films containing ferromagnetic clusters,[43] granular materials,[44–46] and inhomogeneous DMS in the hopping transport regime.[47] In addition to the spin-orbit scattering effect, for granular magnet with a semiconductor host

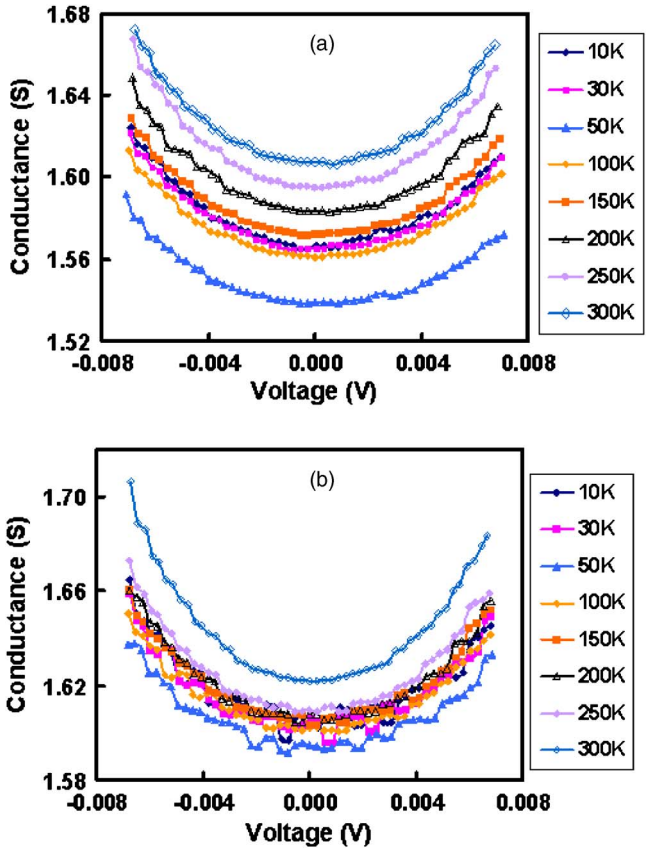

FIG. 7. (Color online) Differential conductance as a function of applied voltage for sample 4: (a) without a field and (b) with an applied magnetic field of 4000 Oe.

matrix, the OHE term may also contain a magnetization-dependent contribution due to the difference between local fields inside the sample and the external field. Although intensive experiments have been carried out on ZnO:Co, so far no report has been made on AHE of this system. Figure 9 shows the Hall resistance as a function of the perpendicular applied magnetic field at 10 K. As can be seen from the figure, the lightly doped samples, samples 2, 3, 6, and 7 exhibit only OHE. However, the heavily doped samples, sample 4 and 8, show clear contributions from both OHE and AHE. In order to understand the origin of AHE in samples 4 and 8, in what follows we will discuss the difference between *M-H* curves obtained by AHE and those measured by SQUID and MCD.

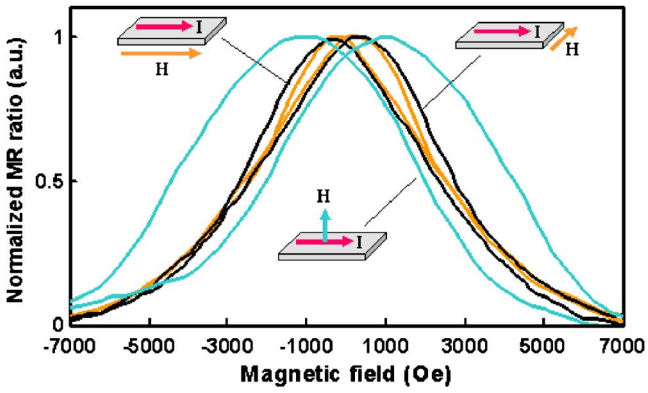

FIG. 8. (Color online) MR curves of sample 4 taken at different applied field directions.

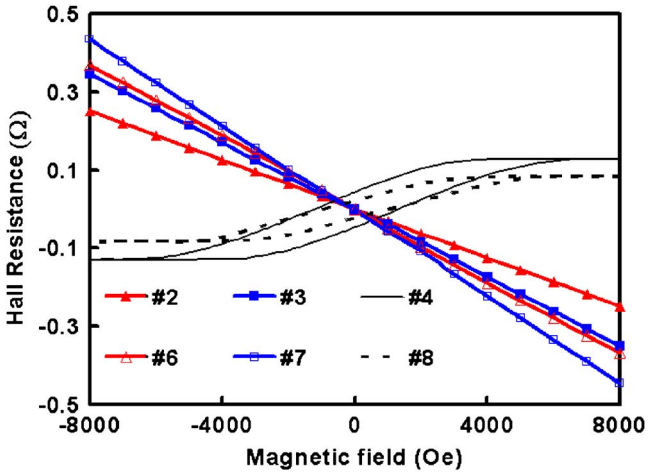

FIG. 9. (Color online) Hall resistance as a function of applied magnetic field for different samples.

E. Comparison between the *M-H* curves obtained by SQUID, MCD, and AHE

As we discussed above, clear hysteresis has been observed in SQUID, MCD, and AHE measurements for samples 4 and 8 [see Figs. 5(a)–5(d)]. The SQUID measurement probes the average magnetic properties of a sample with a size of about 5×5 mm^2. The Hall effect measures the contribution from an area of 324×80 μm^2. Both techniques hence lack the spatial and energy resolutions to discriminate the spurious phases which may confound the data interpretation. Compared to SQUID and Hall effect, MCD is able to detect the presence of different phases due to its photon energy selectivity. This is based on the fact that the MCD signal is proportional to dk/dE, where k is the absorption coefficient and E is the photon energy.[35] Photon energies at which optical transition occurs will be accompanied by a strong MCD response. However, how the MCD will respond to the applied magnetic field at different photon energies will be determined by the nature of the interaction between both the applied magnetic field and magnetic moment of the magnetic impurities with the carriers involved in the optical transition processes. In the case of ZnCoO, there are two energy regions of interest: one is in the band edge absorption region of ZnCoO (or Co-rich secondary phases in heavily doped samples) and the other is in the *d-d* transition region of the Co ions.

As can be seen from Figs. 5(a)–5(d), the MCD data measured at 2.92 eV for sample 4 and 2.8 eV for sample 8 are almost identical in shape compared to those of the respective hysteresis curves measured by SQUID and AHE for the two samples. The agreement is particularly good at room temperature. Considering the fact that the photon energy of 2.92 eV (2.8 eV) is near the band edge absorption of sample 4 (8), as shown in Fig. 3, the good agreement between MCD at this photon energy and the SQUID and AHE data suggests that the magnetic responses are from Co-rich secondary phases. By comparing the hysteresis curves measured by

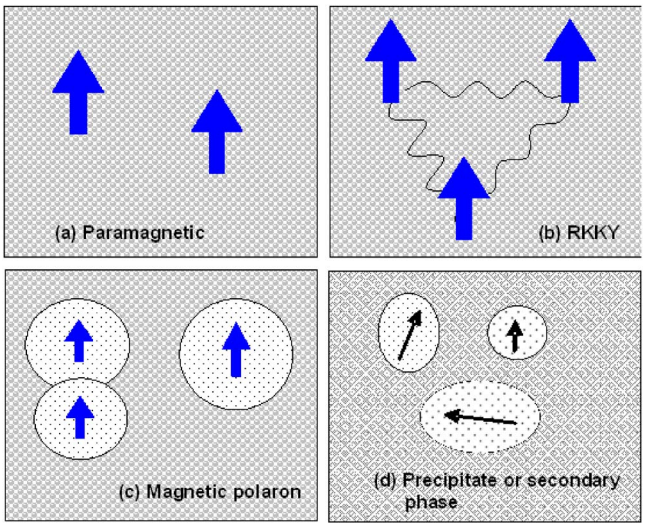

FIG. 10. (Color online) Schematic of different possible sources for magnetism in inhomogeneous DMS systems.

MCD at higher energies as well as those measured by SQUID and AHE, the MCD curves measured at energies in the range of *d-d* transitions are generally slanted more strongly towards the horizontal axis. This suggests that the Co ions which contribute to the *d-d* transitions are mainly from the nonferromagnetic regions (i.e., low Co composition region) in which isolated Co^{2+} ions were found to exhibit anisotropy in the ZnO host matrix. When ferromagnetic interactions exist between these ions, an "easy plane" ferromagnet is expected to form, which may explain the more sheared MCD curves measured at lower energies.[48] The slight difference between the AHE curves with both the MCD (measured at 2.92 eV) and SQUID curves for sample 4 at low temperature can be understood as being caused by additional contribution from nonferromagnetic regions. More detailed studies are being carried out to reveal the difference between the *M-H* curves measured by different techniques.

IV. CONCLUDING REMARKS AND SUMMARY

Based on various results reported so far as well as our systematic study described above, we summarize schematically in Fig. 10 some possible origins of magnetism for the oxide-based DMS. At a very low doping level, there is no or very little interaction among the magnetic dopants; therefore, the system can be considered as either a paramagnet or weak magnet. In the latter case, a small hysteresis might be originated from the interaction between the local spin of *d* electrons and crystal field of the host material. When the dopant concentration further increases, other interactions such as Ruderman-Kittel-Kasuya-Yosida (RKKY), superexchange, and double exchange (in the case of mixed valence) may become possible, and they can either be ferromagnetic or antiferromagnetic, depending on the type and concentration of dopants and charged defects. The ferromagnetic ordering may also occur in very localized regions in the form of magnetic polarons.[49–51] The polarons increase in size when temperature decreases. When they merge, ferromagnetic ordering may occur either locally or globally in the sample. At very high doping levels, it is most likely that clusters of magnetic dopants and/or secondary phases will form. The main difficulty in understating the true mechanism of magnetic ordering in oxide-based DMSs is that, in most cases, all these different phases may coexist. For example, the XRD is unable to differentiate cases (a)–(c) from case (d) (Fig. 10) unless the density and size of the clusters or secondary phases reach certain threshold values. It will be difficult to detect the clusters and secondary phases by conventional TEM when they are either very small or too dilute. The shapes of the *M-H* and magnetization versus temperature curves may have hinted on one mechanism more than the others among the four possibilities, but in reality, most cases fall into the categories (c) and (d). The observation of *d-d* transition in optical spectroscopy is often used to prove that the transition metal dopants substitute for the host cations. However, as we argued above, the observation of *d-d* transition does not necessarily mean that the observed magnetic properties are originated from carrier-mediated ferromagnetic alignment of substitutional magnetic ions. The anomalous Hall effect, in principle, can also originate from any one of the three categories (b)–(d), depending on their density and distribution and electrical properties of both the host matrix and the secondary phases. Based on these background, we believe the observation of hysteresis by AHE, MCD, and SQUID in transition-metal-doped ZnO does not necessarily mean that the material is an intrinsic DMS. When nanoscale inhomogeneity exists, the discussion of the results is meaningful only if the relationships between the structures and properties at nanometer scale are well understood. Recent theoretical efforts have shown that inhomogeneity will form naturally through spinodal decomposition in heavily doped DMSs.[52,53]

In summary, a systematic study has been carried out to investigate the structural, optical, electrical, and magnetic properties of $Zn_{1-x}Co_xO$ ($x=0.05-0.29$) thin films codoped with Al. Although we have observed all the phenomena which are frequently used in literature to conclude the existence of intrinsic ferromagnetism in ZnOCo, we do not believe this is necessarily true unless one can rule out all possible atomic- or cluster-scale inhomogeneities that involve the coexistence of a second phase in the host matrix.

ACKNOWLEDGMENTS

The authors are grateful to Dr. Koji Ando of Nanoelectroncis Research Institute,[53] AIST, Japan for the MCD measurement and detailed analysis of measurement results. The work at the National University of Singapore was supported by the A*-STAR under Grant No. R-398-000-020-305. This work at the University of Michigan was supported by the U.S. National Science Foundation (NSF) under Grant No. DMR 0308012. One of the authors (M.T.) would like to acknowledge the graduate scholarship from A*-STAR.

[1]For review see T. Fukumura, H. Toyosaki, and Y. Yamada, Semicond. Sci. Technol. **20**, S103 (2005); W. Prellier, A. Fouchet, and B. Mercey, J. Phys.: Condens. Matter **15**, R1583 (2003); S. J. Pearton, D. P. Norton, K. Ip, Y. W. Heo, and T. Steiner, J. Vac. Sci. Technol. B **22**, 932 (2004); R. Janisch, P. Gopal, and N. A. Spaldin, J. Phys.: Condens. Matter **17**, R657 (2005).

[2]T. Dietl, H. Ohno, F. Matsukura, J. Cibert, and D. Ferrand, Science **287**, 1019 (2000).
[3]K. Sato and H. Katayama-Yoshida, Jpn. J. Appl. Phys., Part 2 **39**, L555 (2000).
[4]K. Sato and H. Katayama-Yoshida, Jpn. J. Appl. Phys., Part 2 **40**, L334 (2001).
[5]E. C. Lee and K. J. Chang, Phys. Rev. B **69**, 085205 (2004).
[6]N. Spaldin, Phys. Rev. B **69**, 125201 (2004).
[7]M. H. F. Sluiter, Y. Kawazoe, P. Sharma, A. Inoue, A. R. Raju, C. Rout, and U. V. Waghmare, Phys. Rev. Lett. **94**, 187204 (2005).
[8]C. H. Park and D. J. Chadi, Phys. Rev. Lett. **94**, 127204 (2005).
[9]K. Ueda, H. Tabata, and T. Kawai, Appl. Phys. Lett. **79**, 988 (2001).
[10]H. J. Lee, S. Y. Jeong, C. R. Cho, and C. H. Park, Appl. Phys. Lett. **81**, 4020 (2002).
[11]Z. G. Yin, N. F. Chen, C. L. Chai, and F. Yang, J. Appl. Phys. **96**, 5093 (2004).
[12]M. Venkatesan, C. B. Fitzgerald, J. G. Lunney, and J. M. D. Coey, Phys. Rev. Lett. **93**, 177206 (2004).
[13]A. C. Tuan *et al.*, Phys. Rev. B **70**, 054424 (2004).
[14]A. B. Pakhomov, B. K. Roberts, and K. M. Krishnan, Appl. Phys. Lett. **83**, 4357 (2003).
[15]K. Rode, A. Anane, R. Mattana, J.-P. Contour, O. Durand, and R. Lebourgeois, J. Appl. Phys. **93**, 7676 (2003).
[16]M. Bouloudenine, N. Viart, S. Colis, and A. Dinia, Chem. Phys. Lett. **397**, 73 (2004).
[17]Z. Jin, Appl. Phys. Lett. **78**, 3824 (2001).
[18]D. W. Kim, W. J. Cho, and T. W. Kim, J. Mater. Sci. **39**, 4917 (2004).
[19]J. Antony, S. Pendyala, A. Sharma, X. B. Chen, J. Morrison, L. Bergman, and Y. Qiang, J. Appl. Phys. **97**, 10D307 (2005).
[20]J. H. Park, M. G. Kim, H. M. Jang, S. W. Ryu, and Y. M. Kim, Appl. Phys. Lett. **84**, 1338 (2004).
[21]J. H. Kim, H. J. Kim, D. J. Kim, Y. E. Ihm, and W. K. Choo, J. Appl. Phys. **92**, 6066 (2002).
[22]G. Lawes, A. S. Rishbud, A. P. Ramirez, and R. Seshadri, Phys. Rev. B **71**, 045201 (2005).
[23]D. P. Norton *et al.*, Appl. Phys. Lett. **83**, 5488 (2003).
[24]S. C. Wi, Appl. Phys. Lett. **84**, 4233 (2004).
[25]J. C. A. Huang, H. S. Hsu, Y. M. Hu, C. H. Lee, Y. H. Huang, and M. Z. Lin, Appl. Phys. Lett. **85**, 3815 (2004).
[26]Z. Jin, M. Murakami, T. Fukumura, Y. Matsumoto, A. Ohtomo, M. Kawasaki, and H. Koinuma, J. Cryst. Growth **214/215**, 55 (2000).
[27]K. J. Kim and Y. R. Park, Appl. Phys. Lett. **81**, 1420 (2002).
[28]W. Prellier, A. Fouchet, B. Mercey, Ch. Simon, and B. Raveau, Appl. Phys. Lett. **82**, 3490 (2003).
[29]Y.-Z. Yoo, J. Appl. Phys. **90**, 4246 (2001).
[30]T. A. Schaedler, A. S. Gandhi, M. Saito, M. Ruhle, R. Gambino, and C. G. Levi, J. Mater. Res. **21**, 791 (2006).
[31]G. W. Pratt and R. Coelho, Phys. Rev. **116**, 281 (1959).
[32]P. Koidl, Phys. Rev. B **15**, 2493 (1977).
[33]A. Dinia, G. Schmerber, V. Pierron-Bohnes, C. Meny, P. Panissod, and E. Beaurepaire, J. Magn. Magn. Mater. **286**, 37 (2005).
[34]K. Ando, H. Saito, Z. Jin, T. Sukumura, M. Kawasaki, Y. Matsumoto, and H. Koinumab, J. Appl. Phys. **89**, 7284 (2001).
[35]K. Ando, in *Magneto-optics*, Springer Series in Solid-State Science Vol. 128, edited by S. Sugano and N. Kojima (Springer, New York, 1999), p. 211.
[36]M. Paranjape, J. Mitra, A. K. Raychaudhuri, N. K. Todd, N. D. Mathur, and M. G. Blamire, Phys. Rev. B **68**, 144409 (2003).
[37]M. Ziese, Phys. Rev. B **60**, R738 (1999).
[38]S.-S. Yan *et al.* Appl. Phys. Lett. **84**, 2376 (2004).
[39]H. Ohno, Science **281**, 951 (1998).
[40]F. Matsukura, H. Ohno, A. Shen, and Y. Sugawara, Phys. Rev. B **57**, R2037 (1998).
[41]H. Toyosaki, T. Fukumura, Y. Yamada, K. Nakajima, T. Chikyow, T. Hasegawa, H. Koinuma, and M. Kawasaki, Nat. Mater. **3**, 221 (2004).
[42]N. Manyala, Y. Sidis, J. F. DiTusa, G. Aeppli, D. P. Young, and Z. Fisk, Nat. Mater. **3**, 255 (2004).
[43]S. R. Shinde *et al.*, Phys. Rev. Lett. **92**, 166601 (2004).
[44]A. V. Vedyaev, A. B. Granovski, A. V. Kalitsov, and F. Brouers, JETP Lett. **85**, 1204 (1997).
[45]H. Sato, Y. Kobayashi, Y. Aoki, and Y. Yamamoto, J. Phys.: Condens. Matter **7**, 7053 (1995).
[46]B. A. Aronzon, D. Yu. Kovalev, A. N. Lagar'kov, E. Z. Meilikhov, V. V. Ryl'kov, M. A. Sedova, N. Negre, M. Goiran, and J. Leotin, JETP Lett. **70**, 90 (1999).
[47]A. A. Burkov and L. Balents, Phys. Rev. Lett. **91**, 057202 (2003).
[48]P. Sati *et al.*, Phys. Rev. Lett. **96**, 017203 (2006).
[49]T. Dietl, J. Spalek, and L. Swierkowski, Phys. Rev. B **33**, 7303 (1986).
[50]A. Kaminski and S. Das Sarma, Phys. Rev. Lett. **88**, 247202 (2002).
[51]J. M. D. Coey, M. Venkatesan, and C. B. Fitzgerald, Nat. Mater. **4**, 173 (2005).
[52]K. Sato, H. Katayama-Yoshida, and P. H. Dederichs, Jpn. J. Appl. Phys., Part 2 **44**, L948 (2005).
[53]T. Fukushima, K. Sato, H. Katayama-Yoshida, and P. H. Dederichs, Jpn. J. Appl. Phys., Part 2 **45**, L416 (2006).